Substrate Recognition by the Hetero-Octameric ATP Phosphoribosyltransferase from *Lactococcus lactis*†

Karen S. Champagne,‡,§ Elise Piscitelli,|| and Christopher S. Francklyn*,‡,||

Department of Microbiology and Molecular Genetics and Department of Biochemistry, Health Sciences Complex, University of Vermont, B403 Given Building, 89 Beaumont Avenue, Burlington, Vermont 05405

Received August 30, 2006; Revised Manuscript Received October 13, 2006

ABSTRACT: Two families of ATP phosphoribosyl transferases (ATP-PRT) join ATP and 5-phosphoribosyl-1 pyrophosphate (PRPP) in the first reaction of histidine biosynthesis. These consist of a homohexameric form found in all three kingdoms and a hetero-octameric form largely restricted to bacteria. Hetero-octameric ATP-PRTs consist of four $HisG_S$ catalytic subunits related to periplasmic binding proteins and four HisZ regulatory subunits that resemble histidyl-tRNA synthetases. To clarify the relationship between the two families of ATP-PRTs and among phosphoribosyltransferases in general, we determined the steady state kinetics for the hetero-octameric form and characterized the active site by mutagenesis. The K_m^{PRPP} (18.4 ± 3.5 μM) and k_{cat} (2.7 ± 0.3 s^{-1}) values for the PRPP substrate are similar to those of hexameric ATP-PRTs, but the K_m for ATP (2.7 ± 0.3 mM) is 4-fold higher, suggestive of tighter regulation by energy charge. Histidine and AMP were determined to be noncompetitive ($K_i = 81.1$ μM) and competitive ($K_i = 1.44$ mM) inhibitors, respectively, with values that approximate their intracellular concentrations. Mutagenesis experiments aimed at investigating the side chains recognizing PRPP showed that 5′-phosphate contacts (T159A and T162A) had the largest (25- and 155-fold, respectively) decreases in k_{cat}/K_m, while smaller decreases were seen with mutants making cross subunit contacts (K50A and K8A) to the pyrophosphate moiety or contacts to the 2′-OH group. Despite their markedly different quaternary structures, hexameric and hetero-octameric ATRP-PRTs exhibit similar functional parameters and employ mechanistic strategies reminiscent of the broader PRT superfamily.

ATP phosphoribosyltransferase (ATP-PRT,[1] EC 2.4.2.17) catalyzes the first and highly regulated step of histidine biosynthesis, which involves nucleophillic attack of N1 of ATP on C1′ of 5-phosphoribosyl-1 pyrophosphate (PRPP) to form *N*-1-(5′-phosphoribosyl)-ATP (PR-ATP, Figure 1A) (*1*). The resulting product is converted through an additional nine reactions into histidine by a pathway that is regulated both by its end product and by AMP and ADP (*2*). The tight regulation of this pathway (reviewed in ref *3*) reflects the high energetic costs associated with histidine synthesis and the need to dramatically slow pathway flux when histidine is present in the growth media (*4*). Superimposed on top of metabolic control of histidine biosynthesis is genetic regulation of the expression of histidine biosynthetic enzymes, by use of the classic attenuation mechanism (reviewed in ref *5*).

ATP-PRT is a member of the phosphoribosyltransferase (PRT) superfamily of enzymes, all of which share a common chemistry that involves transfer of the phosphoribosyl group to a nucleotide base or, in the case of glutamine phosphoribosyl pyrophosphate amidotransferase, to free ammonia generated on the enzyme (*6*). PRTs are found in many essential pathways, including biosynthesis and salvage of nucleotides and the synthesis of cofactors and amino acids (*7*). There are at least four different structurally unrelated subfamilies of PRTs. Type I PRTs, which include the adenine, orotate (OPRT), and hypoxanthine/guanine PRTs (HGPRT), are composed of four different domains, including a core region that binds both the PRPP and the nucleotide substrate, a hood domain that recognizes the nucleotide substrate, a flexible loop that closes over PRPP, and a C-terminal arm that provides dimerization for some PRTs (*8*). Considerable research attention has focused on the type I PRTs, as the inherited Lesch/Nyan syndrome and orotic aciduria involve respective defects in the HPRT and orotate PRTs (*7*). Other type I PRTs represent targets for therapeutics directed against malaria, Chagas disease, and other pathogenic eukaryotes. Notably, type I PRTs share the PRPP binding motif, a 13-residue signature sequence that is important for substrate recognition (*9*). The type II and type

† This work was supported by NIH Grant GM54899 (C.S.F.) and the Department of Energy Experimental Program to Stimulate Competitive Research (DOE-EPSCOR).

* To whom correspondence should be addressed: Department of Biochemistry, University of Vermont College of Medicine, 89 Beaumont Ave., Burlington, VT 05405. Phone: (802) 656-8450. Fax: (802) 862-8229. E-mail: Christopher.Francklyn@uvm.edu.

‡ Department of Microbiology and Molecular Genetics.

§ Current address: Department of Molecular, Cell, and Developmental Biology, 406 Sinsheimer Labs, University of California, Santa Cruz, CA 95064.

|| Department of Biochemistry.

[1] Abbreviations: AICAR, 5′-phosphoribosyl-4-carboxyamide-5-aminoimidazole; ATP-PRT, ATP phosphoribosyltransferase; PRT, phosphoribosyltransferase; HisRS, histidyl-tRNA synthetase; HPRT, hypoxanthine-guanine phosphoribosyltransferase; OPRT, orotidine phosphoribosyltransferase; QPRT, quinolate phosphoribosyltransferase; PRPP, 5-phosphoribosyl-1-pyrophosphate; PR-ATP, *N*-1-(5′-phosphoribosyl)-ATP.

10.1021/bi061802v CCC: $33.50
Published on Web 11/22/2006

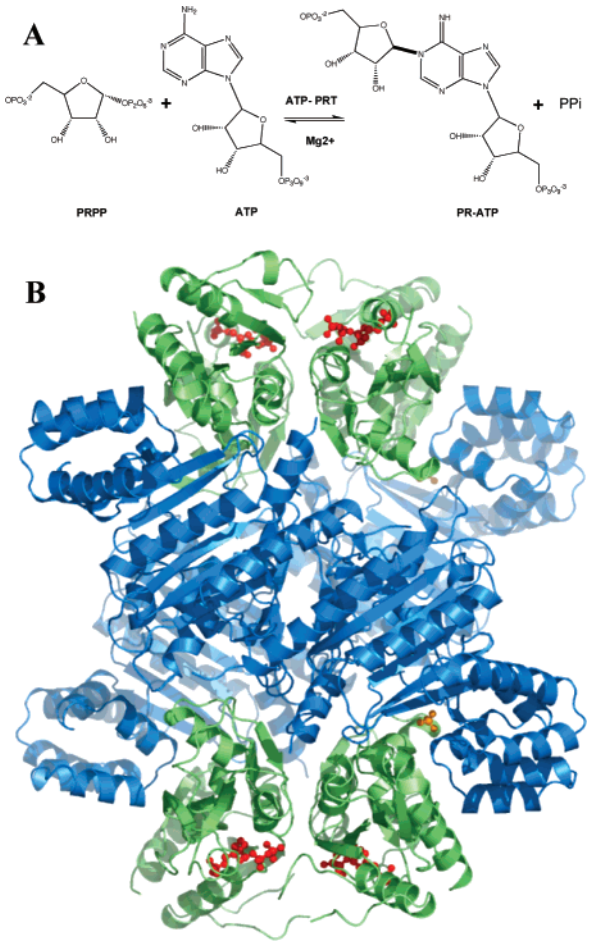

FIGURE 1: ATP phosphoribosyltransferase reaction catalyzed by the hetero-octameric ATP-PRT. (A) Reaction scheme illustrating the nucleophilic attack of N1 from ATP on C1′ of PRPP. (B) Ribbon diagram of the PRPP-bound complex of the hetero-octameric HisZ−HisG PRT from *L. lactis* (*19*). The four $HisG_S$ subunits are colored green, whereas the HisZ subunits are colored cyan. PRPP and inorganic phosphate are rendered in ball-and-stick mode in red and yellow, respectively.

III enzymes are represented by quinolinate (QPRT) and anthranilate PRT, respectively, which participate in NAD^+ and tryptophan biosynthesis (*10*, *11*).

ATP-PRTs represent a fourth class of PRTs and comprise two different subfamilies with distinctly different quaternary structures. The hexameric ATP PRTs, termed $HisG_L$ or long form, are found in enteric bacteria and lower eukaryotes (*12*). Each $HisG_L$ subunit is composed of three domains (*13*, *14*). The first two constitute a mixed α/β bilobal catalytic domain that resembles proteins of the periplasmic binding protein family (*15*), while the third domain provides a binding site to allow feedback inhibition by histidine (*13*). The two different $HisG_L$ structures that are available include a histidine/AMP-inhibited form from *Mycobacterium tuberculosis* (*13*) and an enzyme−product complex of PR-ATP and the enzyme from *Escherichia coli* (*14*). Enzymes from the second ATP-PRT family are hetero-octamers, composed of four $HisG_S$ subunits and four HisZ regulatory subunits (Figure 1B) (*16*, *17*). The latter are structurally related to the catalytic domain of histidyl-tRNA synthetase and provide a regulatory domain to compensate for the absence of the C-terminal domain found in $HisG_L$. Notably, both subunits are required to form a functional complex (*17*). Two structures of the hetero-octameric ATP-PRT have been reported, a histidine-inhibited complex of the enzyme from *Thermatoga maritima* (*18*) and ATP-activated and PRPP-bound forms of the enzyme from *Lactococcus lactis* (*19*).

The sequence conservation between $HisG_S$ and $HisG_L$ indicates a conserved active site and suggests a similarly conserved reaction mechanism (Figure 2). Early work characterizing the steady state kinetics of the long form indicated that the reaction proceeds by an ordered bi-bi mechanism with ATP leading (*20*). Another study involving determination of kinetic isotope effects of the $HisG_L$ enzyme provided evidence that the ATP-PRT transition state has ribo-oxocarbenium character (*21*). In contrast, the kinetic properties of the hetero-octameric form have not yet been characterized. As part of efforts to compare the structure and function of the hexameric and hetero-octameric versions of ATP-PRT, we report here the steady state kinetics of the hetero-octameric HisG/HisZ enzyme from *L. lactis* and a mutational analysis of the contacts between PRPP and the ATP-PRT based on the structure of the activated form of the complex (*19*). Analysis of the resulting mutant proteins highlights the importance of active site contacts with PRPP on ground state binding, as well as the interdependence of the recognition of PRPP, ATP, and the inhibitor histidine.

EXPERIMENTAL PROCEDURES

Construction and Purification of Mutant Proteins. Mutant versions of the *L. lactis* HisZ/HisG ATP-PRT were constructed in the pQE30 expression construct background (*17*). The T159A, T162A, S140A, K8A, K50A, and D155A mutations were introduced by use of the QuikChange mutagenesis procedure (Stratagene). In all cases, the double-stranded primers were 45 nucleotides in length. After mutagenesis, the presence of the directed mutations and the absence of unprogrammed mutations were confirmed by sequencing of the entire genes. The wild-type and all mutant proteins were expressed and purified from *E. coli* overexpression strains by use of a previously published protocol featuring the three-column sequence of Ni-NTA, Superdex 200, and hydroxyapatite chromatography (*16*). Pooled fractions from the final hydroxyapatite column were concentrated to ~6 mg/mL, dialyzed into storage buffer [50 mM Na_2PO_4 (pH 7.5), 300 mM KCl, 10% (v/v) glycerol, and 10 mM β-mercaptoethanol], and then stored at 4 °C for kinetic experiments. Protein concentrations were determined from the extinction coefficient (102 400 M^{-1} cm^{-1}) calculated from the sequences of HisZ and HisG, incorporating a weight average of the two subunit types, as described in ref *16*.

ATP-PRT Assay. The phosphoribosyltransferase activity of ATP-PRT was monitored at A_{290} as an increase in the level of formation of PR-ATP over time (*22*). The measurements were performed at 22 °C in 100 mM Tris-HCl (pH 8.5) containing 10 mM $MgCl_2$, 150 mM KCl, 5 mM β-mercaptoethanol, and 2 units/mL inorganic pyrophosphatase. Purified proteins were added to the indicated concentration, and the reactions were initiated by the addition of PRPP. The absorbance was detected every 9 s for 10 min after initiation of the reaction. The baseline absorbance was established by zeroing the spectrophotometer before adding the PRPP. The extinction coefficient for PR-ATP is 3600 M^{-1} cm^{-1} (*23*), and was used to convert the absorbance units

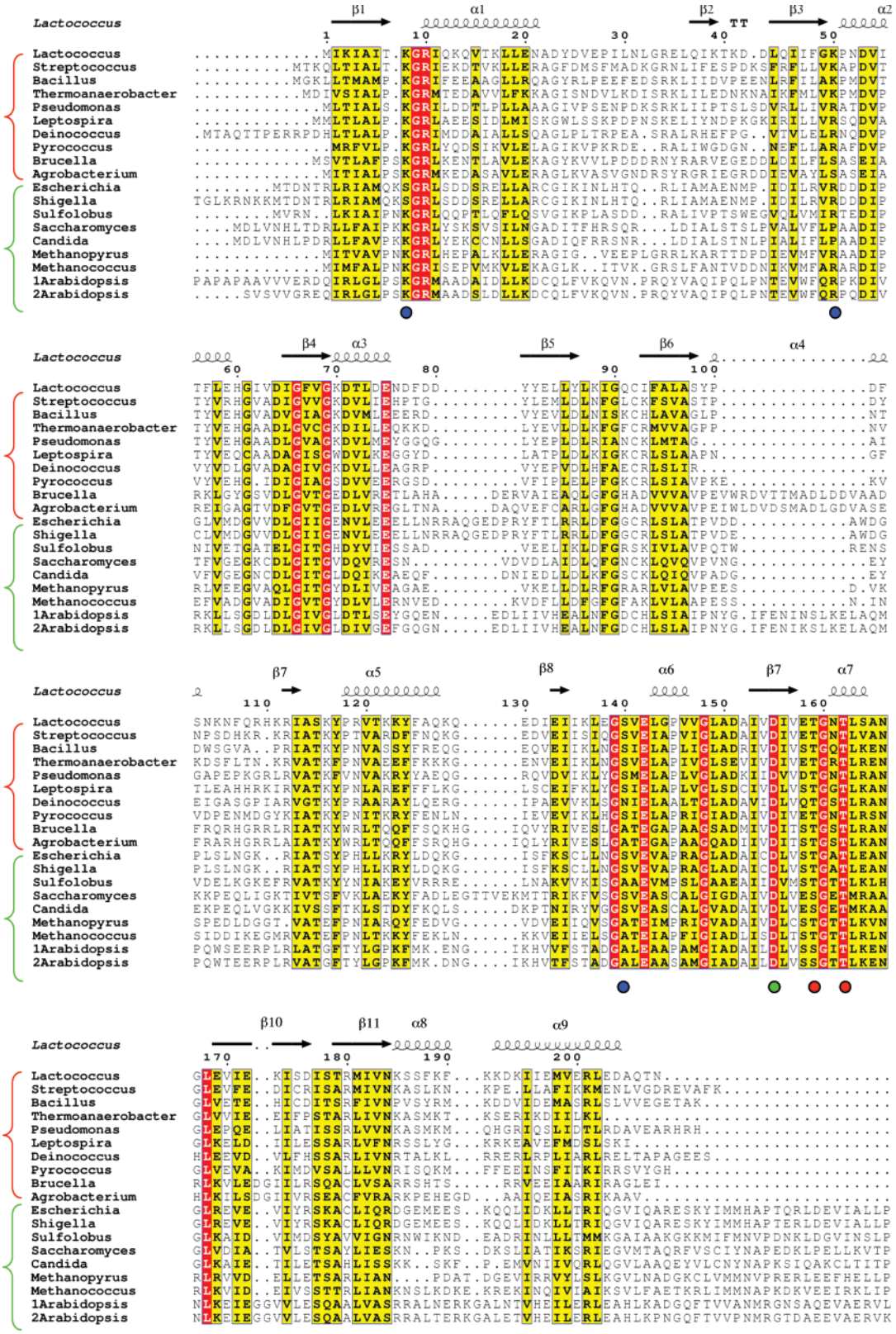

FIGURE 2: Multiple-sequence alignment of representative $HisG_S$ and $HisG_L$ sequences, overlaid with the secondary structure assignments from *L. lactis* $HisG_S$. Sequences corresponding to $HisG_S$ are denoted with red braces, and sequences corresponding to the $HisG_L$ form are denoted with green braces. The alignment omits the histidine binding domain of $HisG_L$, which is absent from $HisG_S$. Blue circles beneath the alignment indicate residues in contact with the pyrophosphate moiety of PRPP, consisting of K8, K50, and S140. The green circle denotes D155. The T159 and T162 side chains are denoted with red circles. The following organisms are included in the alignment: Lactococcus, *L. lactis*; Streptococcus, *Streptococcus mutans*; Thermoanaerobacter, *Thermoanaerobacter tengcongenis*; Pseudomonas, *Pseudomonas aeruginosa*; *Leptospira interrogans* serovar lai str; Deinococcus, *Deinococcus radiodurans*; Pyrococcus, *Pyrococcus furiosus*; Escherichia, *E. coli*; Shigella, *Shigella flexneri*; Sulfolobus, *Sulfolobus solfataricus*; Saccharomyces, *Saccharomyces cerevisiae*; Candida, *Candida albicans*; Methanopyrus, *Methanopyrus kandleri*; Methanococcus, *Methanococcus jannaschii*; Brucella, *Brucella melitensis*; Agrobacterium, *Agrobacterium tumefaciens*; Arabidopsis, *A. thaliana* (there are two isozymes of *A. thaliana*).

per minute to picomoles of product formed per second. Steady state parameters K_m^{PRPP} and K_m^{ATP} were determined by varying the ATP or PRPP concentration while holding the other substrate at a fixed concentration. The PRPP kinetics were measured using a range of 10 μM to 1 mM in PRPP, with 5 mM ATP. For some mutants, the highest concentration of PRPP had to be adjusted upward to accommodate poorer binding. Similarly, the variable ATP assays were performed using ATP concentrations in the range of 100 μM to 5 mM, maintaining the PRPP concentration at 2 mM. The initial rates were calculated from the linear portions of the progress curves, and then the steady state parameters were obtained from saturation plots of $V/[E_o]$ versus [S]. Each substrate concentration was performed three to five times such that the plots were derived using the mean value of $V/[E_o]$. Turnover numbers (k_{cat}) were calculated from the quotient of the maximal catalytic rate divided by the total concentration of active sites. The kinetic parameters for all mutant proteins (except S140A, which proved to be unstable) were measured as described above. The concentrations of the mutant enzymes were adjusted upward when necessary to achieve an initial rate of PR-ATP formation that was approximately equivalent to that of the wild-type enzyme. Reaction mixtures that included inhibitors were prepared by adding AMP or histidine to the 2× reaction buffer and preincubated for 5 min in the presence of enzyme, and then the reactions were initiated by the addition of PRPP. The AMP concentrations employed in the inhibitor assays spanned a range from 0 to 10 mM, while histidine concentrations ranged from 0 to 200 μM.

Data Fitting and Analysis. The kinetic parameters, including K_m and V_{max}, were extracted by directly fitting the initial rate versus substrate data to the Michaelis−Menten equation:

$$V = \frac{V_{max}[S]}{K_m + [S]} \quad (1)$$

This equation was used for experiments involving fixed PRPP and variable ATP concentrations, as well as fixed ATP and variable PRPP concentrations. The data from the histidine and AMP inhibition experiments were plotted as $1/V$ versus $1/[S]$ for each of the four different concentrations of histidine and AMP. The slopes of these lines were used to determine the K_i for histidine and AMP by plotting the K_{mapp}/V_{max} values against histidine or AMP concentration. The slope of the resulting line is equivalent to K_m/K_i, and the abscissa intercept equals the $-K_i$ value for competitive inhibition systems:

$$K_{mapp} = \frac{K_m}{K_i}[I] + K_m \quad (2)$$

RESULTS

Steady State Kinetic Parameters for the PRT Reaction Catalyzed by the Hetero-Octameric ATP-PRTase Reaction. The reaction catalyzed by ATP-PRT and a ribbon diagram of the structure of the *L. lactis* ATP-PRT hetero-octameric complex are presented in Figure 1. As described in Experimental Procedures, the steady state kinetic parameters were determined by use of a continuous assay in which the production of PR-ATP is monitored by the increase in absorbance at 290 nm. Under conditions where the concentration of ATP was fixed at 5 mM and that of PRPP was varied, straightforward Michaelis−Menten behavior was observed, allowing kinetic parameters ($k_{cat} = 2.67 \pm 0.27$ s^{-1} and $K_m^{PRPP} = 18.4 \pm 3.5$ μM) to be readily determined (Figure 3A). The K_m for PRPP for the "short form" enzyme compares reasonably with the values of K_m^{PRPP} determined for "long form" ATP-PRTs (summarized in Table 1), which range from values of 11−67 μM determined for the *Salmonella typhimurium* enzyme (*1*, *20*) to 130 μM determined for the enzyme from *Arabidopsis thaliana* (*24*). This value for K_m^{PRPP} is also comparable to the corresponding

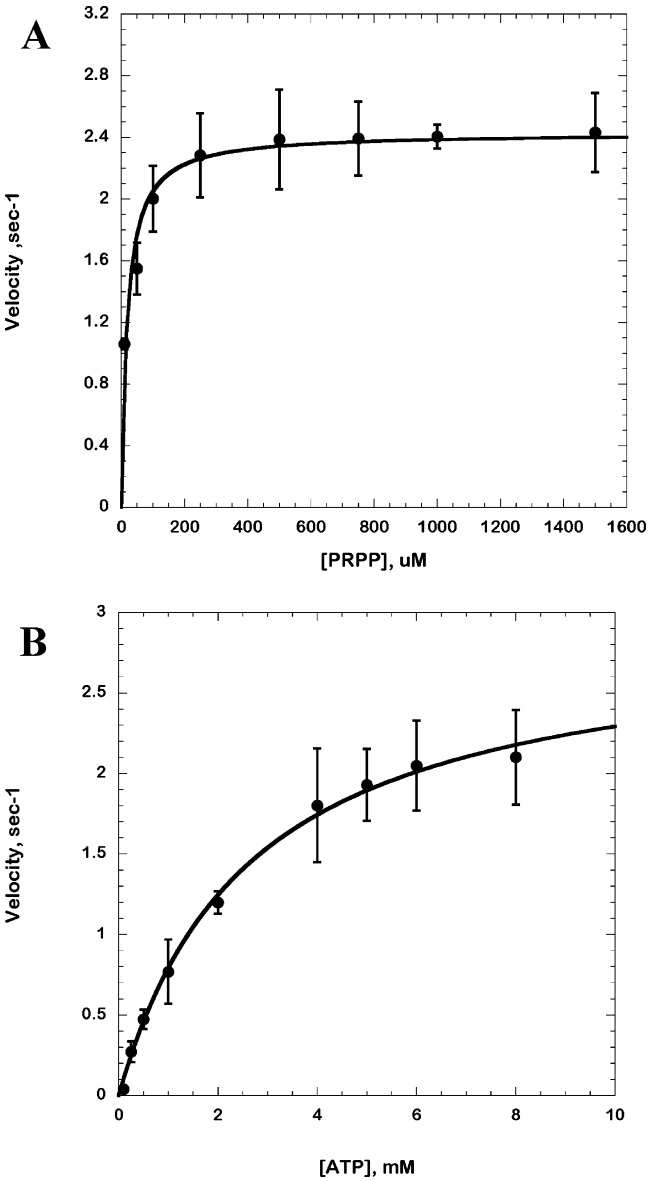

FIGURE 3: Steady state kinetics for wild-type heterooctameric ATP-PRT at 22 °C and pH 8.5. (A) Plot of velocity vs varying concentrations of PRPP, determined at a constant ATP concentration of 5 mM. Wild-type ATP-PRT was added to a final concentration of 24.9 nM. (B) Plot of velocity vs varying ATP concentrations, determined at a constant PRPP concentration of 2 mM. Wild-type ATP-PRT was added to a final concentration of 27.3 nM. The experiments were performed as described in Experimental Procedures. The error bars represent the standard error of the mean for the velocity measurements, which were measured three to five times. The 10−15% errors in the individual measurements were typical for the kinetics of the wild type and all of the mutants reported here.

Table 1: Kinetic Parameters for Hexameric and Hetero-Octameric ATP Phosphoribosyltransferases from Various Species

organism	k_{cat} (s^{-1})	K_m(PRPP) (μM)	K_m(ATP) (mM)	K_i(His) (μM)	K_i(AMP) (mM)	ref
L. lactis	2.67 ± 0.27	18.4 ± 3.5	2.7 ± 0.26	81.1	1.44	this work
T. maritima	ND[a]	ND[a]	ND[a]	350	ND[a]	*18*
S. typhimurium	ND[a]	67	0.2	100	5	*1*
S. typhimurium	2.7	11	0.11	70	5	*20*, *25*
A. thaliana[b]	ND[a]	130/570	0.60/0.51	45/320[c]	ND[a]	*24*

[a] Not determined. [b] Parameter values for the two *A. thaliana* isozymes (ATP-PRT1 and ATP-PRT2) are indicated on either side of the forward slash. [c] Reported as an IC_{50}.

parameters for other PRTs, including the orotate PRT (K_m = 18.7 μM), quinolate PRT (K_m^{PRPP} = 30 μM), and the HPRTs from *Tritrichomonas foetus* (K_m = 46 μM) and *Trypanosoma cruzi* (32.4 μM). Thus, similar Michaelis constants for the PRPP substrate are observed across the entire PRTs superfamily. The level of catalytic activity of the short form ATP-PRT as determined in our assay is comparable to that measured for the long form enzyme from *Salmonella* measured previously (*20*, *25*) but significantly lower than those of the HPRTs from the type I PRT families, which exhibited k_{cat} values in the range of 23−76 s^{-1}. These enzymes lack the complex regulation of ATP-PRT and are invariably dimers. Kinetic parameters were also determined under conditions where PRPP was the constant substrate at 2 mM and ATP was the variable substrate. Over a concentration range of 100 μM to 5 mM in ATP, reliable fits to the Michaelis−Menten equation were obtained, providing the following kinetic parameters: k_{cat} = 2.3 ± 0.25 s^{-1}, and K_m^{ATP} = 2.4 ± 0.24 mM (Figure 3B). Notably, this value is significantly higher than the values of K_M^{ATP} reported for other ATP-PRTs. For example, the K_m^{ATP} for the *S. typhimurium* enzyme was reported as 110−200 μM (*1*, *20*), while values of 600 and 510 μM were determined for the two isozymes of *A. thaliana (24*). Nonphysiological concentrations of ATP in excess of 15 mM were inhibitory to ATP-PRT, which may reflect a competition by ATP for the PRPP binding site, as proposed for AMP (*14*). This phenomenon remains to be investigated in more depth.

Kinetic Parameters of Inhibition by Histidine and AMP. The inhibition of the *L. lactis* enzyme by histidine was determined from velocity versus PRPP concentration plots at a constant ATP concentration of 5 mM, and over histidine concentrations ranging from 0 to 200 μM (Figure 4A). A replot of the slopes of the reciprocal plots against histidine concentration returned a value of 81 μM, indicating that, to a first approximation, histidine is a noncompetitive inhibitor (Figure 4B). This value is in good agreement with early published values (70−100 μM) for the *S. typhimurium* enzyme, but there was an early discrepancy in the literature about whether this inhibition is noncompetitive or uncompetitive (*1*, *26*). Vega et al. (*18*) reported that histidine is a noncompetitive inhibitor of the hetero-octameric *T. maritima* enzyme with a K_i of 350 ± 20 μM, while Ohta et al. reported IC_{50}'s for inhibition by histidine of the *A. thaliana* ATP-PRT1 and ATP-PRT2 of 45 and 320 μM, respectively (*24*). Noncompetitive inhibition by histidine with respect to PRPP for the short form of HisG is consistent with prior data suggesting that the histidine binding site is located in the HisZ subunit, at least 43 Å from C1′ on PRPP where chemistry occurs (*19*). It should be noted that reciprocal plots in Figure 4A appear to intersect below the horizontal axis, which at least formally raises the possibility that the ESI complex has at least a fraction of the activity of the ES complex (*27*). A similar experimental strategy was used to determine the K_i for AMP with PRPP. As determined from the replot in Figure 4D, the K_i for AMP is 1.81 mM and represents competitive inhibition with respect to PRPP. This value is within a factor of 3 of the reported K_i for AMP (5 mM) for the enzyme from *S. typhimurium* (*1*).

Mutations in the PRPP Binding Site Result in a Loss of Catalytic Activity. The similarities in steady state kinetic parameters between the hetero-octameric and hexameric ATP-PRTs, as well as their relationship to the parameters for the more distantly related type I PRTs, motivated a more detailed analysis of the contacts with PRPP suggested by the *L. lactis* crystal structure (Figure 5). The three moieties of PRPP that are directly recognized by the enzyme include the 5′-phosphate, the 2′- and 3′-ribose hydroxyl groups, and the pyrophosphate group (*19*). In both the long and short form enzymes, the 5′-phosphate is recognized by side chains β9 and α7 in HisG, including the main chain amides at T159 and G160, and the γOH groups of T159 and T162. The two latter residues are highly conserved in ATP-PRTs, the only exceptions being the substitution of T159 with serine in the hexameric enzymes from eukaryotes (Figure 2). Pyrophosphate recognition appears to be provided by basic and polar side chains contributed from diverse structural elements, including the β1−α1 loop, the β3−α2 loop, and the N-terminus of α6 (Figure 2). To explore the contributions of these contacts to catalysis in detail, six of the most conserved contacts, including K8, K50, S140, D155, D159, and T162, were substituted with alanine. The resulting mutant proteins were then characterized with respect to their steady state parameters. As indicated in Figure 6 and Table 2, the substitutions that proved to be the most deleterious were those associated with interactions with the 5′-phosphate. The T159A and T162A mutants were both significantly compromised for PRPP binding, with 279- and 49-fold increases in K_m^{PRPP} (Figure 6A,B). In contrast, both mutants were much less affected at the level of k_{cat} (decreased only 2−3-fold relative to that of the wild type) and exhibited slightly decreased values for K_m^{ATP} (Figure 6C,D). These latter parameters indicate that the effect on PRPP binding is likely to be a consequence of the loss of a specific contact and not the result of a global structural defect. The D155A mutant substitutes a carboxylate contact to the 2′-OH group of PRPP that is nearly invariant in both the $HisG_L$ and $HisG_S$ ATP-PRT subfamilies. Of all the mutants tested in the study, D155A was the mutant least affected with respect to enzymatic activity, exhibiting no effect on k_{cat}, and only 3.8- and 1.7-fold increases in the Michaelis constants for PRPP and ATP, respectively (Table 2). Thus, this contact appears to provide an only modest (<0.5 kcal/mol) stabilization of PRPP binding.

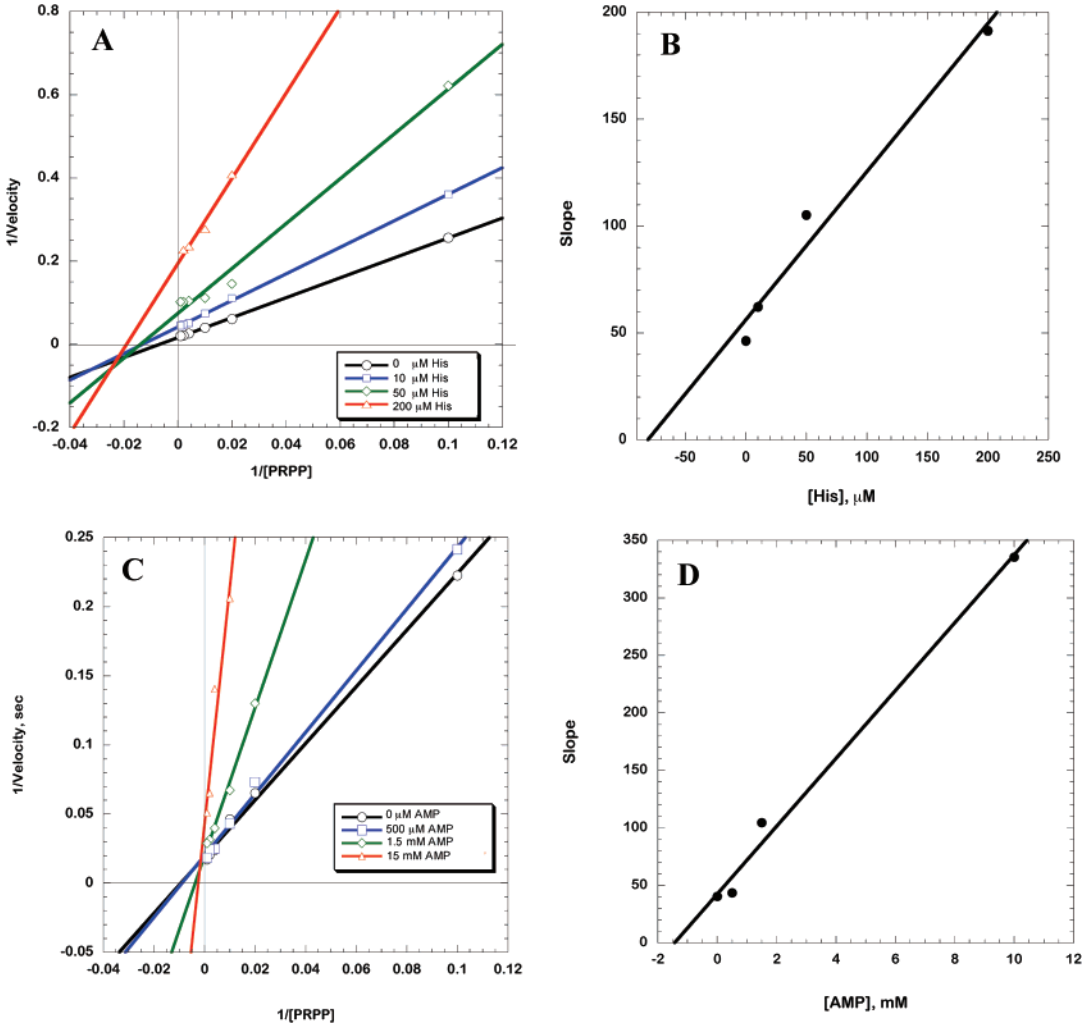

FIGURE 4: Inhibition of ATP-PRT by histidine and AMP. (A) Lineweaver−Burke plots at a range of histidine concentrations from 0 to 200 μM. (B) Replot of the slopes from panel A vs varying histidine concentrations. Wild-type ATP-PRT was added to a final concentration of 39 nM. (C) Lineweaver−Burke plots at a range of AMP concentrations from 0 to 10 mM. (D) Replot of the slopes from panel C, vs varying AMP concentrations. Wild-type ATP-PRT was added to a final concentration of 19.5 nM.

The two side chains in the *L. lactis* complex best positioned to interact with the pyrophosphate group include S140 and K8′. Notably, these are implicated in conformational changes associated with the activation process (*19*). S140 is located in α6, which undergoes a coil to helix transition upon activation, while K8′ makes a relatively long range (~3 Å) cross subunit hydrogen bond to the β-phosphate of the PP_i moiety that is specific to the activated state. A third possible candidate for pyrophosphate interaction is K50′ which, like K8′, also reaches across the dimer interface. Its functional role is less clear from the structure, because it can also make potential interactions with β- and γ-groups of ATP (*19*). All three residues are highly conserved in both the hexameric and hetero-octameric ATP-PRT families; however, K8 and K50 are substituted with serine in some taxa, and S140 is frequently substituted with alanine in the archaeal and eukaryotic versions of $HisG_L$ (Figure 2). In the *L. lactis* enzyme, alanine substitutions of K8′ and K50′ produced stable enzymes that could be readily characterized. The K8A mutant had the milder effect, with a k_{cat} decreased by a modest 2.5-fold, K_m^{ATP} increased 3.5-fold, and K_m^{PRPP} increased 4.5-fold (Table 2). The K50A substitution produced a more substantial effect, causing K_m^{PRPP} and K_m^{ATP} to increase 47- and 2-fold, respectively. Unexpectedly, the

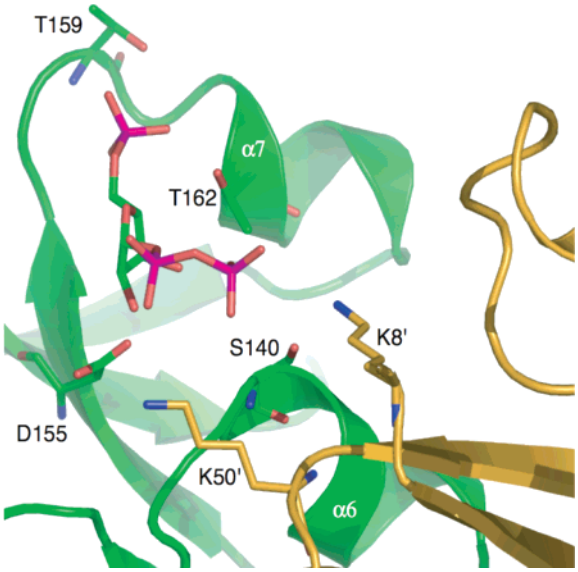

FIGURE 5: PRPP binding site in ATP-PRT from *L. lactis*. The hetero-octameric ATP-PRT active site from the *L. lactis* ATP-PRT complex (*19*) is rendered in ribbon representation, and contacts between PRPP and the enzyme mutated in this study are given. The bound substrate is rendered in stick representation, as are the conserved side chains substituted with alanine in this study.

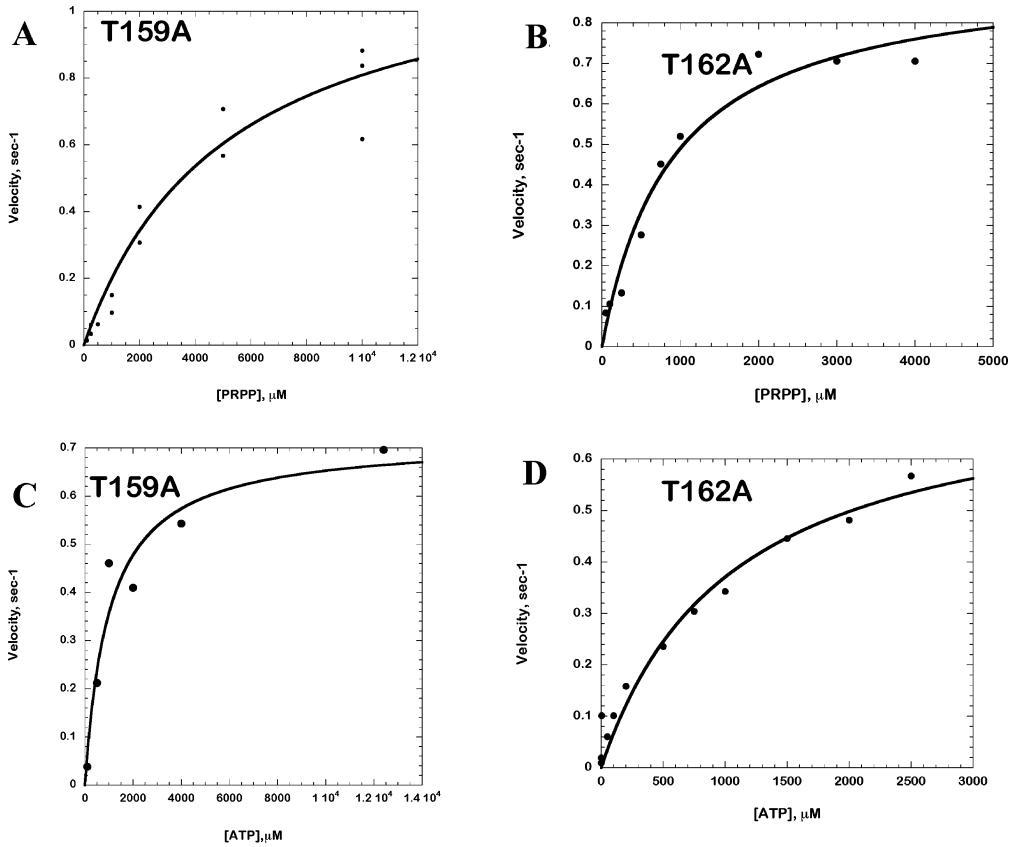

FIGURE 6: Steady state kinetics of PRPP loop mutants T159A and T162A ATP-PRT determined at 22 °C and pH 8.5. (A) Velocity vs PRPP concentration plot for mutant T159A. (B) Plot of velocity vs PRPP concentration for T162A. The mutant enzymes were added to final concentrations of 600 and 100 nM, respectively, for these assays. The PRPP and ATP substrates were at saturating concentrations at 2 and 5 mM, respectively. (C) Velocity vs ATP concentration plot for mutant T159A. (D) Velocity vs ATP concentration plot for mutant T162A. The mutant enzymes were added to final concentrations of 600 and 100 nM, respectively, for these assays. Other details are as noted in the legend of Figure 3.

Table 2: Comparison of ATP-PRT Kinetic Parameters for Wild-Type and Mutant Hetero-Octameric ATP Phosphoribosyltransferases from *L. lactis* at 25 °C and pH 8[a]

	k_{cat} (s^{-1})	K_m(PRPP) (μM)	K_m(ATP) (mM)	k_{cat}/K_m^{PRPP} (M^{-1} s^{-1})
wild type	2.67 ± 0.27	18.4 ± 3.5	2.7 ± 0.26	1.5×10^5
T159A	1.2 ± 0.15	5151 ± 1644	1.07 ± 0.23	2.3×10^2
T162A	0.84 ± 0.08	901 ± 211	1.05 ± 0.31	9.3×10^2
D155A	2.83 ± 0.15	71.2 ± 5.2	4.7 ± 0.79	3.9×10^4
D155A[b]	1.75 ± 0.14	37.6 ± 13.7	ND[c]	4.7×10^4
K8A	1.07 ± 0.02	90 ± 6	8.45 ± 1	1.2×10^4
K50A	6.16 ± 0.48	940 ± 193	5.0 ± 0.7	6.6×10^3
K50A[b]	0.95 ± 0.05	36.3 ± 12	ND[c]	2.6×10^4
S140A[d]	ND[c]	ND[c]	ND[c]	ND[c]

[a] Each value represents the mean and standard deviation of at least three replicates. [b] Parameters determined in the presence of 75 μM histidine. [c] Not determined. [d] This mutant was unstable, and its kinetic parameters could not be determined.

overall k_{cat} for the reaction increased 2.5-fold. Thus, while neither side chain could be said to be essential for catalysis, mutations at both diminished the level of ground state binding to both PRPP and ATP.

All of the aforementioned mutants could be readily expressed and purified, suggesting an absence of obvious effects on protein stability. In contrast, the introduction of the S140A substitution into the *L. lactis* enzyme dramatically weakened expression of $HisG_S$ to the extent that experimentally useful amounts of the S140A hetero-octamer could not be obtained. Attempts to detect any PRT activity in the residual amount of complex that could be captured by the Ni-NTA column were unsuccessful, and the subunit stoichiometry of the eluted material could not be determined. Accumulation of the regulatory HisZ subunit did not seem to be affected by the mutation, suggesting that each subunit is not strictly dependent on the other for the preservation of stability. At a minimum, these results suggest that S140 plays an essential role in the the folding of $HisG_S$ or serves to stabilize the quaternary structure of the octamer. From these results alone, the potential role of S140 in catalysis could not be assessed.

Coupling of Histidine-Mediated Inhibition to Substrate Binding by ATP-PRT. In our published model to account for the effect of histidine on ATP-PRT function, the binding of histidine to a site on the HisZ subunit causes a rearrangement of the HisZ−$HisG_S$ interface, which is ultimately relayed through secondary structure elements to the side

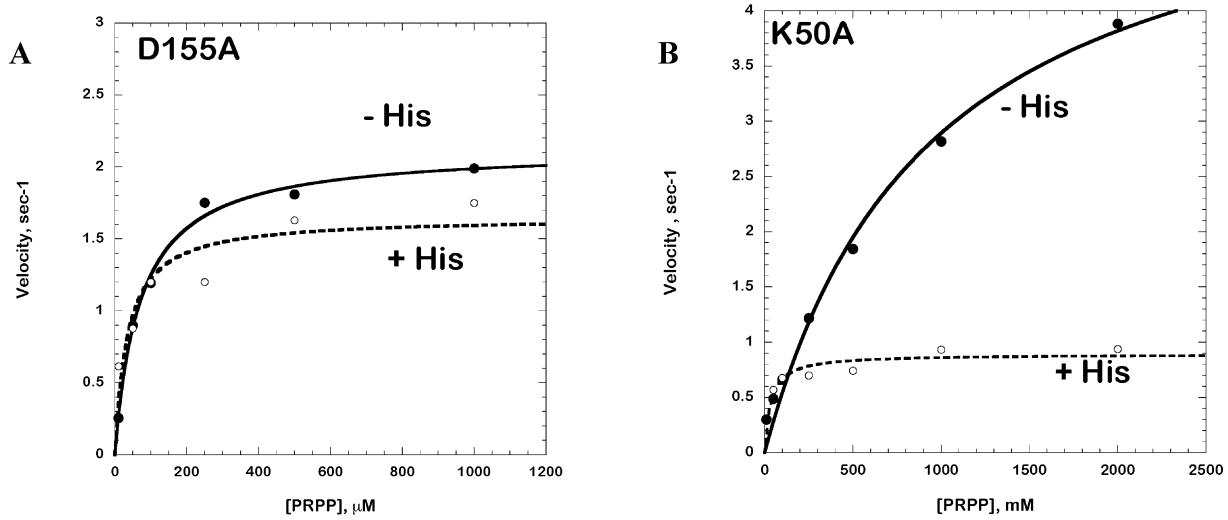

FIGURE 7: Steady state kinetics of D155A and K50A mutants of *L. lactis* ATP-PRTase determined at 22 °C and pH 8.5. (A) Velocity vs PRPP concentration plot for D155A, in the presence (○) or absence (●) of 75 μM histidine. The mutant enzyme was added to a final concentration of 23.4 nM for these assays. (B) Velocity vs PRPP concentration for K50A, in the presence (○) or absence (●) of 75 μM histidine. The mutant enzyme was added to a final concentration of 31.25 nM for these assays. For both enzymes, saturating concentrations of PRPP and ATP substrates were 2 and 5 mM, respectively. Other details are as noted in the legend of Figure 3.

chains that directly contact PRPP (*19*). As a first test of this model, we compared the sensitivity of two different mutants, D155A and K50A, to the presence of 75 μM histidine, a concentration nearly equivalent to K_i for the wild-type enzyme. These two side chains were selected to provide a comparison between a residue with a predicted role in allosteric transmission to one with no obvious connection to the predicted structural pathway for histidine inhibition. For the former, K50A is located at the amino terminus of $HisG_S$ α2, an α-helix whose C-terminal end is located in the $HisG_S$ dimeric interface that abuts HisZ. In our model, binding of histidine to HisZ is expected to transmit structural changes to the ATP-PRT binding site via the HisZ−HisG interface and α2. In contrast, D155 is a highly conserved residue on β9 that contacts the 2′-OH group of PRPP but is not connected to a secondary structure element that undergoes a conformational change upon histidine binding. In the presence of 75 μM histidine, the kinetic parameters for D155A and K50A were both altered, indicating that the effect of histidine binding has not been completely uncoupled in either mutant (Table 2). The magnitudes of the perturbations were, however, significantly different for the two mutants. Histidine at a concentration of 75 μM had a comparatively modest effect on D155A, as k_{cat} and K_m^{PRPP} were decreased by factors of only 1.6- and 1.9-fold, respectively (Figure 7A). In contrast, the k_{cat} parameter was decreased 6.8-fold, and K_m^{PRPP} was decreased 25.8-fold for the K50A mutant (Figure 7B). For both mutants, therefore, the presence of histidine increased the affinity of the enzyme for PRPP and decreased the overall k_{cat}. The comparatively greater change in parameters for the K50A mutant is consistent with its proposed involvement in the transduction of the allosteric signal associated with histidine binding. However, the enhancement of PRPP binding seen in the presence of histidine for K50A provides some of the first direct kinetic evidence of the structural relationship between substrate and inhibitor binding and underscores the complex nature of regulation in this system.

DISCUSSION

The Biological Basis for ATP-PRT Kinetic Parameters: Optimization in Response to Intracellular Substrate and Inhibitor Concentrations. The original studies on ATP-PRT were motivated by an appreciation of its importance in biosynthetic regulation. These studies estimated the energetic cost of histidine biosynthesis in *S. typhimurium* to be on the order of ~41 ATPs, representing a substantial physiological burden (*28*). More recently, a genome scale modeling analysis of total *E. coli* physiology highlighted the ATP-PRT reaction as one of a limited number of key biosynthetic reactions that are thermodynamically unfavorable yet essential for bacterial growth (*29*). These empirical and theoretical observations illustrate why selective pressures may have led to complex regulatory features in ATP-PRT that allow it to control histidine biosynthesis at the metabolic level. The principal goal of this study was to explore the functional differences of the two distinct forms of ATP-PRT, both of which appear to share a common evolutionary ancestry (*12*) yet possess different quaternary structures (*13*, *14*, *18*, *19*). Identification of functional features that separate the two classes should help to account for their persistence in contemporary organisms.

A comparison of the parameters for the hetero-octameric enzyme with those for the hexameric enzymes indicates that, on balance, similarities outweighed differences. The value of K_m^{PRPP} determined for the *L. lactis* enzyme (18.4 ± 3.5 μM) is similar to the values determined for the hexameric prokaryotic enzymes but lower than the values for the two isoforms of *A. thaliana* (Table 1). Notably, the Michaelis constants for PRPP for the two ATP-PRT classes in prokaryotic enzymes are significantly lower than the estimated intracellular concentration of PRPP in *S. typhimurium*, which has been measured to be 350 μM (*30*). Under typical physiological conditions, therefore, the hexameric and hetero-octameric forms of the enzyme would both be expected to be saturated with PRPP, providing little regulation by this substrate. However, the intracellular PRPP pool is likely to

vary in a complex fashion in response to the summed contribution of the fluxes through the histidine and purine biosynthesis pathways (*31*). In addition to sharing PRPP as a common precursor, both pathways share 5′-phosphoribosyl-4-carboxyamide-5-aminoimidazole (AICAR) as a common intermediate, providing a direct basis for additional integration. It is therefore not surprising that the K_m^{PRPP} reported here for the ATP-PRTs is similar in magnitude to the Michaelis constants for PRPP determined for other PRTs in nucleotide biosynthesis and salvage pathways (*32*), including OPRT (*33*), QPRT (*34*), and HGPRT (*32*). Thus, the size of the PRPP pool is likely to regulate histidine biosynthesis by virtue of the competition between ATP-PRT and the other enzymes in the nucleotide and amino acid biosynthetic pathways that employ PRPP as a substrate.

The long and short forms similarly exhibit nearly identical noncompetitive K_i's for histidine, in the range of 70−100 μM. This value lies between the intracellular concentration of histidine in cells growing on media lacking histidine (25 μM) and cells growing in the presence of 50 μg/mL histidine (100 μM), suggesting that both forms of ATP-PRT are "tuned" to be maximally responsive to changes in histidine concentration over a relatively tight but biologically significant concentration range (*3*). Not surprisingly, the value of K_i^{His} detemined here is nearly equal to the histidine Michaelis constant for histidyl-tRNA synthetase ($K_m^{His} = 35$ μM), which possesses a structurally similar binding pocket (*35*). In view of the structural differences between the histidine binding domains of the two enzyme families (*13*, *14*, *18*, *19*), this nearly identical value of the K_i for histidine for the long and short forms is striking. The higher K_i^{His} (350 μM) reported for the *T. maritima* enzyme (*18*) represents a significant outlier from these values but could be a consequence of performing the measurement at 20 °C, which is below the physiologically optimal temperature for *Thermatoga* of 80 °C. It is notable that the two isoforms of ATP-PRT in *A. thaliana*, which may be located in different intracellular compartments, differ significantly with respect to their IC_{50}'s for histidine (*24*). Histidine biosynthesis for this organism may be under different control in the cytoplasm and chloroplast, but definitive proof that ATP-PRT controls histidine flux in plants has not yet been reported.

While the parameters for PRPP and histidine were essentially identical between the two ATP-PRT families, K_m^{ATP} differed by a factor of more than 10 (Table 1). The K_m^{ATP} for the long form enzyme is significantly below the intracellular concentration of ATP of 3 mM (*36*), while that of the short form enzyme is approximately equal to it. Early work by Atkinson and co-workers showed that the regulation of the hexameric ATP-PRT by energy charge is sensitized in the presence of histidine (*37*, *38*), consistent with the synergistic binding effects of histidine and the competitive inhibitor AMP indicated from kinetic and structural analysis. The higher value of K_m^{ATP} for the hetero-octameric enzyme could reflect a requirement for tighter regulation of ATP-PRT by energy charge in the absence of histidine, a possibility that remains to be addressed in future work. Intriguingly, the presence of histidine increased the k_{cat}/K_m^{PRPP} for K50A to a value within a factor of 5 of that of the wild type (Table 2 and Figure 7). This suggests that the K50A mutation unmasks the structural linkage between substrate and histidine binding, perhaps as a consequence of the direct role of this residue in the allosteric pathway. Preliminary results from an investigation of HisZ−HisG interface mutants (E. Piscitelli and C. S. Francklyn, unpublished results) reveal similar behavior, underscoring the complex relationship between substrate and inhibitor binding.

Implications for the Mechanism of the ATP-PRT Reaction. The principal points of contact on PRPP for ATP-PR active site side chains include the 5′-phosphate, the 2′- and 3′-ribose hydroxyls, and the pyrophosphate group (Figure 5). In our published model for the activation of the ATP-PRT reaction, secondary structure elements responsible for recognition of the 5′-phosphate and 2′- and 3′-ribose hydroxyls of PRPP undergo minimal conformational change in response to substrate binding, while those that interact with the pyrophosphate group must be mobilized from sequestered locations in the structure during the activation process (*19*). In particular, the highly conserved PRPP loop does not undergo any structural changes during the activation process, so its interactions with PRPP would be expected to provide relatively uniform binding across the reaction coordinate. Consistent with this prediction, we found that T159A and T162A increased K_m^{PRPP} but had relatively minor effects on k_{cat} (Table 2). The D155A mutant had a qualitatively similar, but smaller, effect. Contacts with the 5′-phosphate and the 2′-OH group are therefore likely to represent essentially ground state interactions. This is consistent with the competitive nature of AMP binding with respect to both PRPP and ATP, which appears to be stabilized by interactions between the 5′-phosphate and the conserved PRPP loop (*14*).

Early kinetic isotope work indicated that the transition state for ATP-PRT has significant dissociative character, suggesting that the bond to the leaving group is lengthened considerably before appreciable bond formation to the nucleophile has occurred (*21*). Here, we examined the potential role of leaving group stabilization by mutating K8, K50, and S140, the basic and or polar side chains that represent the most likely candidates for interactions with the pyrophosphate moiety upon activation. None of these, however, decreased k_{cat} to a significant extent, arguing against the idea that neutralizing interactions between these basic side chains and the negatively charged pyrophosphate group strengthen as the reaction approaches the transition state. (The role of interactions by S140 could not be assessed because of the instability of the resulting mutant protein.) However, K8A and K50A increased K_m^{PRPP}, and K50A was in fact associated with a modest increase in k_{cat}. If K50A is important for uniform binding to PRPP and ATP over the entire reaction coordinate, a weaker interaction with the PR-ATP product might be expected to accelerate the rate of product release. Similar observations were made with regard to the effects of the K68E mutant in *Tr. cruzii* HPRT on K_m^{PRPP} and k_{cat} (*39*). Like K8 and K50 in ATP-PRT, K68 is implicated in pyrophosphate binding in HPRT. In both systems, therefore, interactions with the pyrophosphate moiety may therefore be contributing uniform binding free energy to catalysis, as opposed to differential stabilization to the transition state (*40*). These observations argue against the idea that chemistry is rate-limiting for the overall reaction but are consistent with the general observation that, for many PRTs, product release is the rate-determining step (*6*).

Detailed analysis of the transition states for nucleoside phosphorylase (*41*) and OPRT (*42*) suggests that an important

feature of the PRT mechanism is the concept of "nucleophilic displacement" (*6*). For nucleoside phosphorylase, this involves relatively fixed interactions with the nucleobase leaving group and P_i nucleophile, but a clear migration of C1′ (on the order of 3 Å) from the leaving group to the P_i nucleophile. For both of these enzymes, a significant number of the electrostatic interactions that serve to stabilize the transition state are intramolecular and are not provided by direct interactions with active site chains. For example, the developing positive charge on O4′ in the ribooxocarbenium ion is stabilized by negative charges contributed from the 5′-phosphate and Mg^{2+}−pyrophosphate moieties. Achieving this stabilization requires a specific geometry in the substrate that is enforced by the enzyme active site, which also prevents solvent water molecules from attacking the reactive species like the oxocarbenium ion. If this view is a reasonable picture of the ATP-PRT mechanism, then the principle contribution the enzyme makes to enhance the rate of catalysis is to limit conformational and translational freedom in the substrates, thereby lowering the free energy of activation. Such a view could explain the absence of obvious "catalytic" residues in ATP-PRT whose substitution would be expected to diminish k_{cat} by significant factors of $>2-3$ orders of magnitude (*43*).

While ATP-PRTs and type I PRTs are defined by structurally unrelated catalytic domains, functionally homologous active site loops and secondary structure elements can be identified that appear to underlie similarities in mechanism. Thus, the PRPP loop of type I PRTs, with its characteristic pair of acidic residues and conserved TXXT motif, can be readily superimposed (rmsd = 0.5−0.8 Å) on the PRPP loop of ATP PRTs (*14*). Recognition of the pyrophosphate group by type I PRTs is mediated by two elements, the "PP_i loop" found between β1 and α2 that exhibits minimal sequence conservation (save for a rare non-proline cis peptide between the first and second residues of the loop) and the "flexible loop", a conformationally mobile structural element that is only ordered when the Mg^{2+}−PRPP moiety is bound in the active site. Notably, mutagenesis studies on type I PRTs focusing on the PP_i and flexible loops have been reported and indicate that, like our results with K8A and K50A, substitutions of PRPP-contacting residues preferentially increase K_m^{PRPP} without imposing significant effects on k_{cat} (*39*, *44*). In a study that correlated mutations in human HPRT with various in vitro and in vivo phenotypes, among the recurring mutations were substitutions that affected residues responsible for binding Mg^{2+}, which is coordinated to the pyrophosphate (*45*). One perplexing issue not yet addressed in any of the ATP-PRT structure studies or the work reported here is the absence of information concerning Mg^{2+} binding. Divalent metal is required for activity, but there is no structural evidence for it in any of the complexes reported thus far. As yet, none of the available ATP-PRT crystal structures has provided information about the pattern of Mg^{2+} binding in the type IV enzyme, so similarities in metal binding cannot be assessed. This important question remains to be addressed in future studies.

ACKNOWLEDGMENT

We thank Ethan Guth and Robert Hondal for useful discussions and comments on the manuscript and Tim Hunter of the Vermont Cancer Center DNA Sequencing Facility for DNA analysis services.

REFERENCES

1. Martin, R. G. (1963) The first enzyme in histidine biosynthesis: The nature of feedback inhibition by histidine, *J. Biol. Chem. 238*, 257−68.
2. Morton, D. P., and Parsons, S. M. (1977) Inhibition of ATP phosphoribosyltransferase by AMP and ADP in the absence and presence of histidine, *Arch. Biochem. Biophys. 181*, 643−8.
3. Winkler, M. E. (1987) Biosynthesis of Histidine, in *Escherichia coli and Salmonella Typhimurium. Cellular and Molecular Biology* (Neidhardt, F. C., Ed.) pp 395−411, American Society for Microbiology, Washington, DC.
4. Ames, B. N., Martin, R. G., and Garry, B. J. (1961) The first step of histidine biosynthesis, *J. Biol. Chem. 236*, 2019−26.
5. Blasi, F. (1976) Gene expression of the histidine operon, *Acta Microbiol. Acad. Sci. Hung. 23*, 151−9.
6. Schramm, V. L., and Grubmeyer, C. (2004) Phosphoribosyltransferase mechanisms and roles in nucleic acid metabolism, *Prog. Nucleic Acid Res. Mol. Biol. 78*, 261−304.
7. Musick, W. D. (1981) Structural features of the phosphoribosyltransferases and their relationship to the human deficiency disorders of purine and pyrimidine metabolism, *CRC Crit. Rev. Biochem. 11*, 1−34.
8. Smith, J. L. (1999) Forming and inhibiting PRT active sites, *Nat. Struct. Biol. 6*, 502−4, 706 (erratum).
9. Sinha, S. C., and Smith, J. L. (2001) The PRT protein family, *Curr. Opin. Struct. Biol. 11*, 733−9.
10. Kim, C., Xuong, N. H., Edwards, S., Madhusudan, Yee, M. C., Spraggon, G., and Mills, S. E. (2002) The crystal structure of anthranilate phosphoribosyltransferase from the enterobacterium *Pectobacterium carotovorum*, *FEBS Lett. 523*, 239−46.
11. Sharma, V., Grubmeyer, C., and Sacchettini, J. C. (1998) Crystal structure of quinolinic acid phosphoribosyltransferase from *Mycobacterium tuberculosis*: A potential TB drug target, *Structure 6*, 1587−99.
12. Bond, J. P., and Francklyn, C. (2000) Proteobacterial histidine-biosynthetic pathways are paraphyletic, *J. Mol. Evol. 50*, 339−47.
13. Cho, Y., Sharma, V., and Sacchettini, J. C. (2003) Crystal structure of ATP phosphoribosyltransferase from *Mycobacterium tuberculosis*, *J. Biol. Chem. 278*, 8333−9.
14. Lohkamp, B., McDermott, G., Campbell, S. A., Coggins, J. R., and Lapthorn, A. J. (2004) The structure of *Escherichia coli* ATP-phosphoribosyltransferase: Identification of substrate binding sites and mode of AMP inhibition, *J. Mol. Biol. 336*, 131−44.
15. Wang, Z., Luecke, H., Yao, N., and Quiocho, F. A. (1997) A low energy short hydrogen bond in very high resolution structures of protein receptor−phosphate complexes, *Nat. Struct. Biol. 4*, 519−22.
16. Bovee, M. L., Champagne, K. S., Demeler, B., and Francklyn, C. S. (2002) The quaternary structure of the HisZ-HisG N-1-(5′-phosphoribosyl)-ATP transferase from *Lactococcus lactis*, *Biochemistry 41*, 11838−46.
17. Sissler, M., Delorme, C., Bond, J., Ehrlich, S. D., Renault, P., and Francklyn, C. (1999) An aminoacyl-tRNA synthetase paralog with a catalytic role in histidine biosynthesis, *Proc. Natl. Acad. Sci. U.S.A. 96*, 8985−90.
18. Vega, M. C., Zou, P., Fernandez, F. J., Murphy, G. E., Sterner, R., Popov, A., and Wilmanns, M. (2005) Regulation of the hetero-octameric ATP phosphoribosyl transferase complex from *Thermotoga maritima* by a tRNA synthetase-like subunit, *Mol. Microbiol. 55*, 675−86.
19. Champagne, K. S., Sissler, M., Larrabee, Y., Doublie, S., and Francklyn, C. S. (2005) Activation of the hetero-octameric ATP phosphoribosyl transferase through subunit interface rearrangement by a tRNA synthetase paralog, *J. Biol. Chem. 280*, 34096−104.
20. Morton, D. P., and Parsons, S. M. (1976) Biosynthetic direction substrate kinetics and product inhibition studies on the first enzyme of histidine biosynthesis, adenosine triphosphate phosphoribosyltransferase, *Arch. Biochem. Biophys. 175*, 677−86.
21. Goitein, R. K., Chelsky, D., and Parsons, S. M. (1978) Primary ^{14}C and a secondary ^{3}H substrate kinetic isotope effects for some phosphoribosyltransferases, *J. Biol. Chem. 253*, 2963−71.
22. Voll, M. J., Appella, E., and Martin, R. G. (1967) Purification and composition studies of phosphoribosyladenosine triphosphate:

pyrophosphate phosphoribosyltransferase, the first enzyme of histidine biosynthesis, *J. Biol. Chem. 242*, 1760−7.
23. Ames, B. N., Hartman, P. E., and Jacob, F. (1963) Chromosomal alterations affecting the regulation of histidine biosynthetic enzymes in *Salmonella*, *J. Mol. Biol. 7*, 23−42.
24. Ohta, D., Fujimori, K., Mizutani, M., Nakayama, Y., Kunpaisal-Hashimoto, R., Munzer, S., and Kozaki, A. (2000) Molecular cloning and characterization of ATP-phosphoribosyl transferase from *Arabidopsis*, a key enzyme in the histidine biosynthetic pathway, *Plant Physiol. 122*, 907−14.
25. Kleeman, J. E., and Parsons, S. M. (1976) Reverse direction substrate kinetics and inhibition studies on the first enzyme of histidine biosynthesis, adenosine triphosphate phosphoribosyltransferase, *Arch. Biochem. Biophys. 175*, 687−93.
26. Whitfield, H. J., Jr. (1971) Purification and properties of the wild type and a feedback-resistant phosphoribosyladenosine triphosphate pyrophosphate phosphoribosyltransferase, the first enzyme of histidine biosynthesis in *Salmonella typhimurium*, *J. Biol. Chem. 246*, 899−908.
27. Segel, I. (1975) *Enzyme Kinetics: Behavior and analysis of rapid equilibrium and steady state kinetics*, Wiley, New York.
28. Brenner, M., and Ames, B. N. (1971) The histidine operon and its regulation, in *Metabolic Regulation* (Voge, H. J., Ed.) Academic Press, New York.
29. Hatzimanikatis, V., Li, C., Ionita, J. A., Henry, C. S., Jankowski, M. D., and Broadbelt, L. J. (2005) Exploring the diversity of complex metabolic networks, *Bioinformatics 21*, 1603−9.
30. Sadler, W. C., and Switzer, R. L. (1977) Regulation of *Salmonella* phosphoribosylpyrophosphate synthetase activity in vivo. Deductions from pool measurements, *J. Biol. Chem. 252*, 8504−11.
31. Pendyala, L., and Wellman, A. M. (1975) Effect of histidine on purine nucleotide synthesis and utilization in *Neurospora crassa*, *J. Bacteriol. 124*, 78−85.
32. Munagala, N., Basus, V. J., and Wang, C. C. (2001) Role of the flexible loop of hypoxanthine-guanine-xanthine phosphoribosyltransferase from *Tritrichomonas foetus* in enzyme catalysis, *Biochemistry 40*, 4303−11.
33. Wang, G. P., Lundegaard, C., Jensen, K. F., and Grubmeyer, C. (1999) Kinetic mechanism of OMP synthase: A slow physical step following group transfer limits catalytic rate, *Biochemistry 38*, 275−83.
34. Cao, H., Pietrak, B. L., and Grubmeyer, C. (2002) Quinolinate phosphoribosyltransferase: Kinetic mechanism for a type II PRTase, *Biochemistry 41*, 3520−8.
35. Francklyn, C., Adams, J., and Augustine, J. (1998) Catalytic Defects in Mutants of Class II Histidyl-tRNA Synthetase from *Salmonella typhimurium* Previously Linked to Decreased Control of Histidine Biosynthesis Regulation, *J. Mol. Biol. 280*, 847−58.
36. Neuhard, J., and Nygaard, P. (1987) *Biosynthesis and Conversions of Nucleotides*, Vol. 1, American Society for Microbiology, Washington, DC.
37. Klungsoyr, L., and Atkinson, D. E. (1970) Regulatory properties of phosphoribosyladenosine triphosphate synthetase. Synergism between adenosine monophosphate, phosphoribosyladenosine triphosphate, and histidine, *Biochemistry 9*, 2021−7.
38. Klungsoyr, L., Hagemen, J. H., Fall, L., and Atkinson, D. E. (1968) Interaction between energy charge and product feedback in the regulation of biosynthetic enzymes. Aspartokinase, phosphoribosyladenosine triphosphate synthetase, and phosphoribosyl pyrophosphate synthetase, *Biochemistry 7*, 4035−40.
39. Canyuk, B., Medrano, F. J., Wenck, M. A., Focia, P. J., Eakin, A. E., and Craig, S. P., III (2004) Interactions at the dimer interface influence the relative efficiencies for purine nucleotide synthesis and pyrophosphorolysis in a phosphoribosyltransferase, *J. Mol. Biol. 335*, 905−21.
40. Albery, W. J., and Knowles, J. R. (1976) Evolution of enzyme function and the development of catalytic efficiency, *Biochemistry 15*, 5631−40.
41. Fedorov, A., Shi, W., Kicska, G., Fedorov, E., Tyler, P. C., Furneaux, R. H., Hanson, J. C., Gainsford, G. J., Larese, J. Z., Schramm, V. L., and Almo, S. C. (2001) Transition state structure of purine nucleoside phosphorylase and principles of atomic motion in enzymatic catalysis, *Biochemistry 40*, 853−60.
42. Tao, W., Grubmeyer, C., and Blanchard, J. S. (1996) Transition state structure of *Salmonella typhimurium* orotate phosphoribosyltransferase, *Biochemistry 35*, 14−21.
43. Kraut, D. A., Carroll, K. S., and Herschlag, D. (2003) Challenges in enzyme mechanism and energetics, *Annu. Rev. Biochem. 72*, 517−71.
44. Page, J. P., Munagala, N. R., and Wang, C. C. (1999) Point mutations in the guanine phosphoribosyltransferase from *Giardia lamblia* modulate pyrophosphate binding and enzyme catalysis, *Eur. J. Biochem. 259*, 565−71.
45. Duan, J., Nilsson, L., and Lambert, B. (2004) Structural and functional analysis of mutations at the human hypoxanthine phosphoribosyl transferase (HPRT1) locus, *Hum. Mutat. 23*, 599−611.

BI061802V